Automatika

Journal for Control, Measurement, Electronics, Computing and Communications

ISSN: (Print) (Online) Journal homepage: https://www.tandfonline.com/loi/taut20

Investigation on extendable multiport DC–DC boost converter for hybrid renewable energy systems

M. Anish John Paul, C. Agees Kumar & J. Jerusalin Carol

To cite this article: M. Anish John Paul, C. Agees Kumar & J. Jerusalin Carol (2021) Investigation on extendable multiport DC–DC boost converter for hybrid renewable energy systems, Automatika, 62:3-4, 486-502, DOI: 10.1080/00051144.2021.1985704

To link to this article: https://doi.org/10.1080/00051144.2021.1985704

Published online: 07 Oct 2021.

AUTOMATIKA
2021, VOL. 62, NOS. 3–4, 486–502
https://doi.org/10.1080/00051144.2021.1985704

Investigation on extendable multiport DC–DC boost converter for hybrid renewable energy systems

M. Anish John Paul[a], C. Agees Kumar[b] and J. Jerusalin Carol[c]

[a]Department of EEE, Mar Ephraem College of Engineering and Technology, Elavuvilai, India; [b]Department of EEE, Arunachala College of Engineering for Women, Vellichanthai, India; [c]Department of CSE, Mar Ephraem College of Engineering and Technology, Elavuvilai, India

ABSTRACT

In this work, the integration of renewable hybrid energy (RHE) resources using extendable multiport DC–DC boost converter is investigated. Three renewable energy sources such as solar photovoltaic (PV) system, wind energy system and fuel cell (FC) are integrated into the grid via this converter and grid-tied inverter. The output voltage of the multiport DC–DC boost converter is controlled using adaptive neuro fuzzy inference system-based controller. The overall system model is developed and tested in the MATLAB simulation software and also implemented in real time. The overall system is tested for different operating conditions such as change in irradiance condition of the solar PV panel, change in wind speed condition of the wind turbine, change in hydrogen pressure conditions of the FC and sudden change in load conditions and corresponding results are measured and analysed. The efficiency of the proposed system is about 98.21%. Finally, experimental results of the proposed model are also presented to examine the suitability of the system.

ARTICLE HISTORY
Received 9 January 2021
Accepted 21 September 2021

KEYWORDS
Three-input step-up DC–DC converter (TISUC); wind turbine (WT); photovoltaic (PV); fuel stack (FS); grid; renewable energy resources (RES)

Nomenclature

RHE	Renewable Hybrid Energy
DC	Direct Current
ANFIS	Adaptive Neuro Fuzzy Inference System
TISUC	Three-Input Step-up DC–DC Converter
WT	Wind Turbine
FS	Fuel Stack
MPPT	Maximum Power Point Tracking
RES	Renewable energy resources
TWH	Terawatt Hour
FC	Fuel Cell
VER	Variable Energy Sources
AC	Alternating Current
PMSG	Permanent Magnet Synchronous Generator
PWM	Pulse Width Modulation

1. Introduction

The need for electrical power is extremely important due to an increase in world population, residents and industries. Earlier time, the electrical energy is generated by means of fossil fuels. But fossil fuels always created the problem for the environment and also disturbed the ecological structure of the world. To overcome this problem, renewable source of energy and nuclear energy are vital alternative sources for fossil fuels.

Renewable energy resources (RES) are used in most countries due to their increasing usage in all applications. Till now, 34.6% of using renewable energy sources was installed in India. These resources are frequently employed since they are efficient and inexpensive, and also the overall amount of energy consumption is increasing daily. In 2018, India generated 1487 TWH of total electricity. However, every year, the demand for electricity rises by 12%. Even though renewable sources are not reliable, it is sustainable. So to be reliable, the proposed hybrid system provides excellent solution for future electricity demand. Both solar and wind power generation systems are best sources, which brings the CO_2 level down from the atmosphere.

In the future, dispersed energy systems would need interfacing unique varieties of power resources. Fuel cells (FC), wind turbines (WT) and photovoltaic (PV) systems may proceed as appropriate options for assuaging the aforesaid issues concerning delivery of nearby electric power load for customers, gratitude toward their reduced current spending then and non-appearance of transmission losses. Separate power delivery as of those sources is not cost-effective because of small depending ability and excessive initial costs. Therefore, the above-mentioned inadequacies may be quite determined via combining those sources with linking them to the utility grid.

CONTACT C. Agees Kumar ageesofficials@gmail.com

Interfacing renewable energy sources to the grid [1] are proposed for operators and policymakers to address. Variable energy sources (VER) are renewable energy sources that combine wind and solar to produce electricity. While the costs of solar and wind continue to fall dramatically and wind and solar are becoming cheaper than traditional sources of energy in many places, reliability issues related to greater penetration of VER are challenging to conventional networks.

The power produced through these renewable resources always varies with environmental conditions. Due to this, the voltage at output of the renewable energy sources also varies. DC link voltage should be maintaining at specified level when renewable energy sources are integrated with grid. In general, renewable energy sources can connect directly to a grid-tied inverter if the voltage across the renewable energy sources meets the needed voltage level for grid integration. When the voltage across renewable energy sources is low, it is impossible to integrate with the grid and a DC–DC boost converter is necessary to bring the low voltage to the desired level [2,3]. Conventional DC–DC boost converters have the problem of operating at high duty cycles to boost the voltage, putting a lot of stress on the power semiconductor devices used in the DC–DC boost converter, lowering overall efficiency and limiting voltage gain [4–7]. Literature relevant to the DC–DC boost converter is as follows.

To improve the converter's efficiency, a wireless sensors-based CMOS switched-capacitor DC–DC converter was presented in [8]. Three different gain topologies were used to configure the CMOS converter. With a switching frequency of 12 Mega Hertz, the proposed scheme had an efficiency of around 85%.

Generally, grid-tied inverters were utilized to connect several renewable energy sources to the grid using independent DC–DC converters [9]. This technique necessitated independent control for each DC–DC converter, and as a result of the control scheme, an instability problem in the hybrid renewable energy system can arise. References [10,11] presented a single-stage DC–AC converter with multiple input energy sources. Similar issues arise as a result of this type of organization as well. To tackle this, a multiport converter model for integrating hybrid renewable energy sources into the grid has been proposed [12–15].

Several-port converters like those seen in [16–21] are useful for integrating multiple power sources with varying energy capacities to get a controlled output voltage. The issue with that setup is that, in order to avoid power coupling, only one power source is authorized to transmit power into the load at a time. In [22], a bidirectional multi-input port converter for merging battery and FC sources for electric vehicle applications was presented. This converter is typically incompatible with a variety of renewable energy sources. According to the findings of this literature review, a high voltage gain DC–DC multi-input port converter is required for the effective integration of hybrid renewable energy sources into the grid, as well as an effective voltage controller for the high voltage gain DC–DC multi-input converter to maintain the power flow between various RES. The goal of this project is to fill these research gaps. Based on these research gaps, the objectives of this work are given as:

(1) For hybrid renewable energy sources such as solar PV, wind energy and FC systems, the design and development of an extendable multi-input step-up converter are presented in this work.
(2) In this work, an adaptive neuro fuzzy inference system (ANFIS)-based DC link voltage controller is presented to keep the DC link voltage at a set level for the improved operation of hybrid renewable energy sources.

The following is a breakdown of the paper's structure:

Section 2 describes the overall system of the proposed three-input step-up DC–DC boost converters fed hybrid renewable energy system, Section 3 describes the simulation results and their discussions of the system's performances, Section 4 describes the proposed system's real-time implementation and Section 5 concludes with some remarks.

2. Multiport DC–DC boost converter for hybrid renewable energy systems

The general block diagram of the Multiport DC–DC boost converter for Hybrid renewable energy systems is shown in Figure 1(a). A three-input step-up converter is included in the proposed system, which is fed from a hybrid energy system such as solar PV, FCs, or wind energy.

The maximum power point tracking (MPPT) controller measures and processes the voltage and current of PV panels. The duty cycle is generated by the MPPT controller and processed by the pulse width modulation (PWM) generator. To extract the peak power out of the solar PV panel, the PWM generator sends a pulse to the S1 switch of the three-input port step-up converter. The MPPT controller measures and processes the FC voltage and current. The duty cycle is generated by the MPPT controller and processed by the PWM generator. To extract the peak power out of the FC, the PWM generator sends a pulse to the S2 switch of the three-input port step-up converter. The MPPT controller measures and processes the voltage and current of the wind generator rectifier. The duty cycle is generated by the MPPT controller and processed by the PWM generator. To extract the maximal power from the WT, the pulse from the PWM generator is sent to the S3 switch of the three-input port step-up converter.

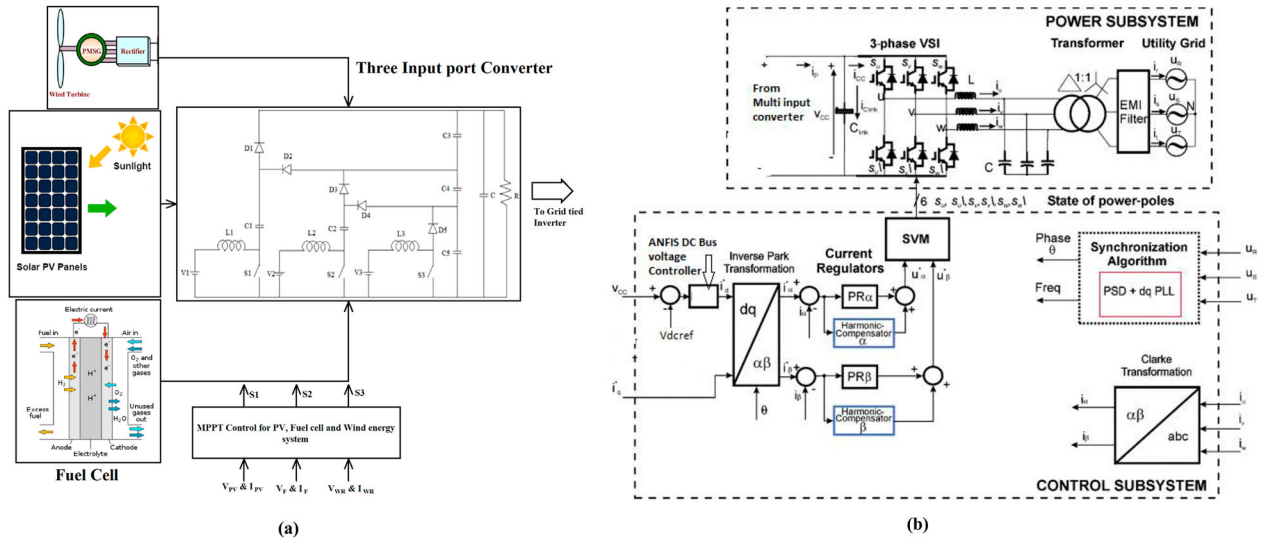

Figure 1. (a) Multiport DC–DC boost converter for Hybrid renewable energy systems and (b) grid integration of Multiport DC–DC boost converter for hybrid renewable energy systems.

The overall block diagram of the Grid integration of Multiport DC–DC boost converter for Hybrid renewable energy systems is shown in Figure 1(b). The output of the three-input port DC–DC step-up converter is connected to the DC–AC inverter input. The DC–AC converter's output is connected to the grid via a harmonic filter. For the DC–AC inverter, the D-Q control technique is used. The grid voltage is processed via phase locked loop for generating phase sequence (θ). The DC–AC converter's DC link voltage (V_{cc}) was measured and compared to a reference voltage (V_{dcref}). The ANFIS processes the error voltage, and the ANFIS controller provides direct axis reference current (I_d*) for the next stage. The inverse park transformation converts direct and quadrature axis reference current (I_d* and I_q*) to reference alpha and beta current ($I_\alpha*$ and $I_\beta*$). By using the clarke transformation, the actual grid current (i_u, i_v, i_w) is turned into alpha and beta current (I_α and I_β). The reference and actual alpha and beta current are compared and processed via PR controller. The PR controller generates the controlled voltage signal ($u_\alpha*$ and $u_\beta*$). This control signal is processed using space vector modulation to generate pulses for the DC–AC inverter, and it regulates power flow from renewable energy sources to load and grid, as well as grid to load, based on renewable energy sources' power availability.

2.1. Wind turbine (WT)

Figure 2 depicts the WECS investigated in this study. The working of the WECS is defined by the following system parameters such as wind speed (v_w), diode bridge output voltage (V_{dc}) and mechanical speed (ω_m).

In Figure 2, the power $P_T(v_w, \omega_m)$ reflects the power captured by the WT after friction losses are taken into account. The permanent magnet synchronous generator (PMSG) absorbs some of this power, while the balance adjusts the shaft speed (P_J). $P_{em}(\omega_m, V_{dc})$ is the electromagnetic power that enters the PMSG. The electromagnetic power $P_{em}(\omega_m, V_{dc})$ is separated into the resistive losses induced by the PMSG and the line, $P_R(\omega_m, V_{dc})$, and the diode bridge output power, $P_0(\omega_m, V_{dc})$, while ignoring the machine's magnetic losses and the bridge's diode losses. Finally, the converter receives the majority of the power $P_0(\omega_m, V_{dc})$ [20].

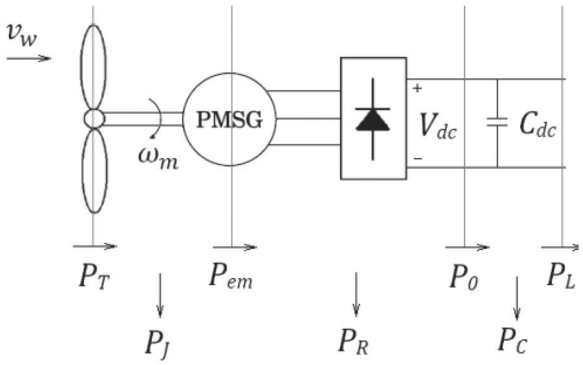

Figure 2. Equivalent circuit diagram of PMSG-based wind energy system.

2.2. PV array

The equivalent circuit diagram of PV cell is exposed in Figure 3.

A solar cell is generally made up of a power supply and an inverted diode connected in parallel. It uses series and parallel resistors to represent series and parallel connections, respectively. A disruption in the direction of electron migration from the n to p junction causes series resistance, while leakage currents cause parallel resistance [13].

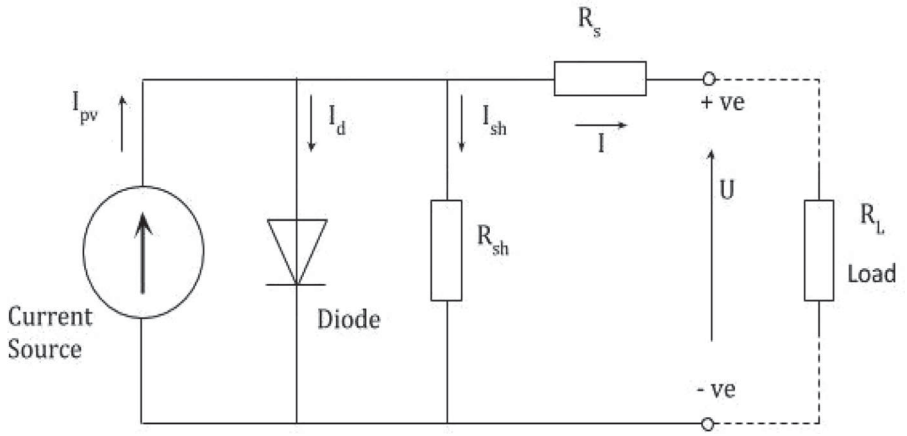

Figure 3. Equivalent circuit of a solar cell.

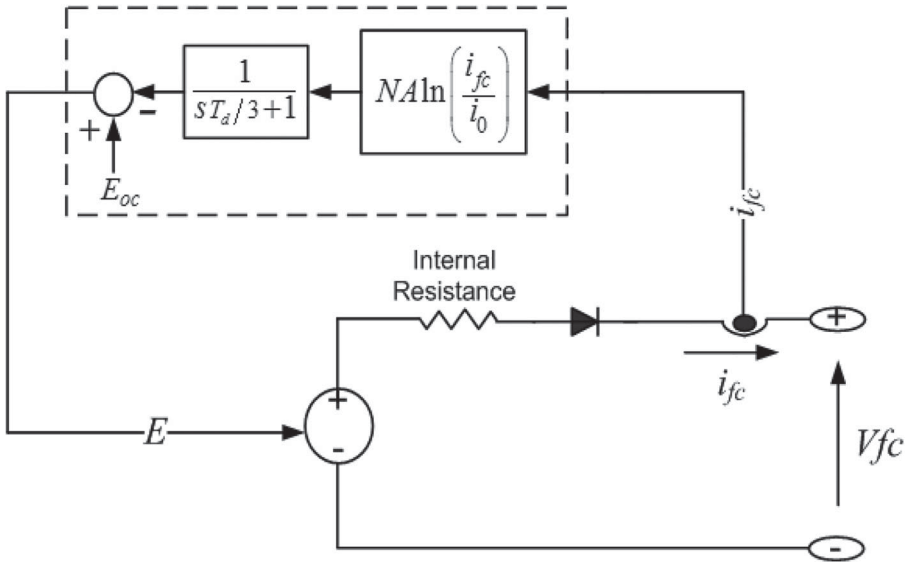

Figure 4. Equivalent circuit diagram of FS cell.

The PV current at the output end is represented in the following equation:

$$I = I_{\text{scc}} - I_{\text{d}} \tag{1}$$

$$I_{\text{d}} = I_{\text{O}}\left(e^{\frac{qV_{\text{d}}}{KT}} - 1\right) \tag{2}$$

where the reciprocal of the diode current saturation is denoted by I_{o}, the current od short circuit in PV panel is denoted by I_{scc}, the current through the diode is denoted by I_{d}, electron of charge is denoted by q, voltage across of the diode is denoted by V_{d}, Boltzmann constant ($1.38 * 10^{-19}$ J/K) denoted by k and the temperature at junction is denoted by T in degree kelvin (K).

By solving Equations (1) and (2)

$$I = I_{\text{scc}} - I_{\text{o}}\left(e^{\frac{qV_{\text{d}}}{kT}} - 1\right) \tag{3}$$

By proper estimates,

$$I = I_{\text{scc}} - I_{\text{o}}\left(e^{q\left(\frac{V+IRs}{nKT}\right)} - 1\right) \tag{4}$$

where PV cell current is denoted by I, PV cell voltage is denoted by V and diode ideality factor is denoted by n.

2.3. FC stack design

The equivalent circuit diagram of the fuel stack (FS) is displayed in Figure 4.

Water vapour anode pressure is considered to be 50% of saturated vapour pressure, whereas water cathode pressure is assumed to be 100%. The product is in the liquid phase and the FC runs at 100°C. The basic model signifies a specific gasoline mobile stack working on insignificant circumstances of temperature and strain. Based on the polarization curve obtained from the producer data sheet, the parameters of the equal circuit may be modified. A diode is used to prevent negative current from flowing into the stack. A FC stack generates a DC output with a low voltage and high current [15].

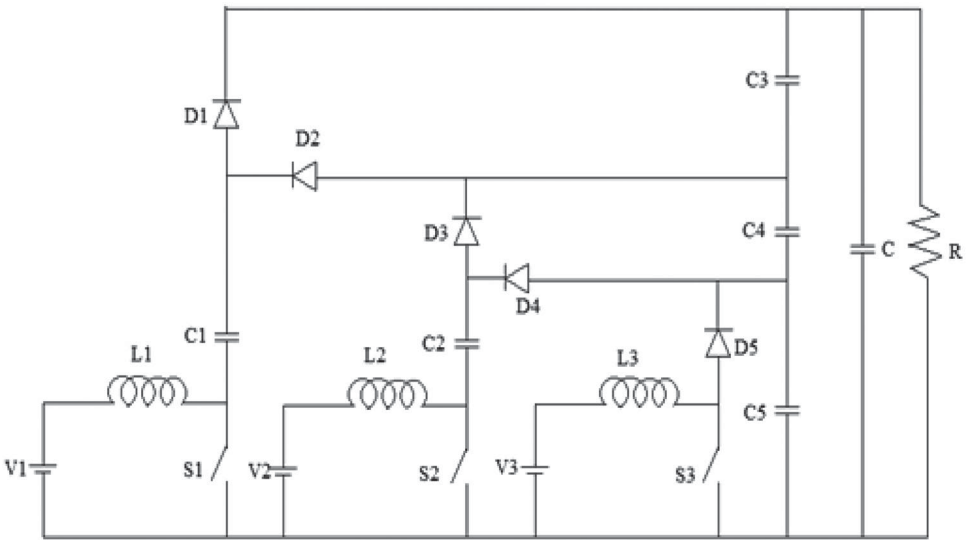

Figure 5. Circuit diagram three-input step-up converter.

2.4. Design of three-input port step-up converter for hybrid energy system

Figure 5 depicts the proposed three-input port step-up converter for a hybrid energy system. The three-input sources are controlled by the power semiconductor switches S1, S2 and S3. Inductors and capacitors operated as converter filtering components, while diodes were utilized to freewheel the current during the off state of the power semiconductor switch [23].

The three-input port step-up converter's steady-state output voltage across the load "*R*" is provided by

$$V_{\mathrm{O}} = \sum_{J=1}^{3} \frac{V_j}{1 - d_j} \tag{5}$$

where three-input step-up converter output voltage is denoted by V_{o}, each input port voltage is denoted by and power semiconductor switch S1, S2 and S3 operating duty cycle is denoted by d_j.

2.4.1. Modes of operation of the three-input step-up converter

There should be some overlapping time between the ON states of the power switches for normal converter operation. The switching signals of the input cell switches that are charging the even-numbered capacitors are interleaved with 180° phase shift with the switching signals of the input cell switches, which are charging the odd-numbered capacitors.

According to Figure 5, the first and third inputs charge the odd-numbered capacitors, and their switches (S1 and S2) have the same switching pattern, while the second input charges the even-numbered capacitors, and the second input switching signal has a 180° phase shift with the S1 and S2 switching signals. The duty cycles of the switches are assumed to be equal for presenting the operating modes of the proposed converter.

Figure 6(a) depicts the gating signal for the switches S1, S2 and S3. The converter operation in different mode such as mode 1, mode 2 and mode 3 is shown in Figure 6(b–d).

Mode 1: All of the power switches S1, S2 and S3 are turned on in this mode (see Figure 6(b)). The input voltages charge the three inductors L1, L2 and L3, and their currents rise linearly. All the diodes are biased reversely, and also, they are not conducting; therefore, the voltage of all the capacitors except the output capacitor remains constant. The output load is supplied by the output capacitor in this mode 1.

Mode 2: The primary and second switches S1and S2 are both on in this mode, but the third switch S3 is off. Diodes D2, D4 and D5 are forward biased and diodes D1 and D3 are reverse biased. The third inductor L3's current charges the even-numbered capacitors C2, C4 while discharging the odd-numbered capacitors C1, C3, C5. The load is supplied by the output capacitor C.

Mode 3: Power switches S1 and S2 are turned off, while power switch S3 is turned on. Diodes D2, D4 and D5 are reverse biased and the diodes D1 and D3 are forward biased. The current flowing through the primary and secondary inductors L1 and L2 is used to charge the odd-numbered capacitors C1, C3, C5 and discharge the even-numbered capacitors C2, C4. The load and output capacitors are supplied by the ultimate input inductor L3.

2.4.2. Design of inductor and capacitor

The average current of the inductors can be expressed as

$$i_{\mathrm{L1,avg}} = \frac{M}{1 - d_1} I_{\mathrm{out}} \tag{6}$$

$$i_{\mathrm{L2,avg}} = \frac{M}{1 - d_2} I_{\mathrm{out}} \tag{7}$$

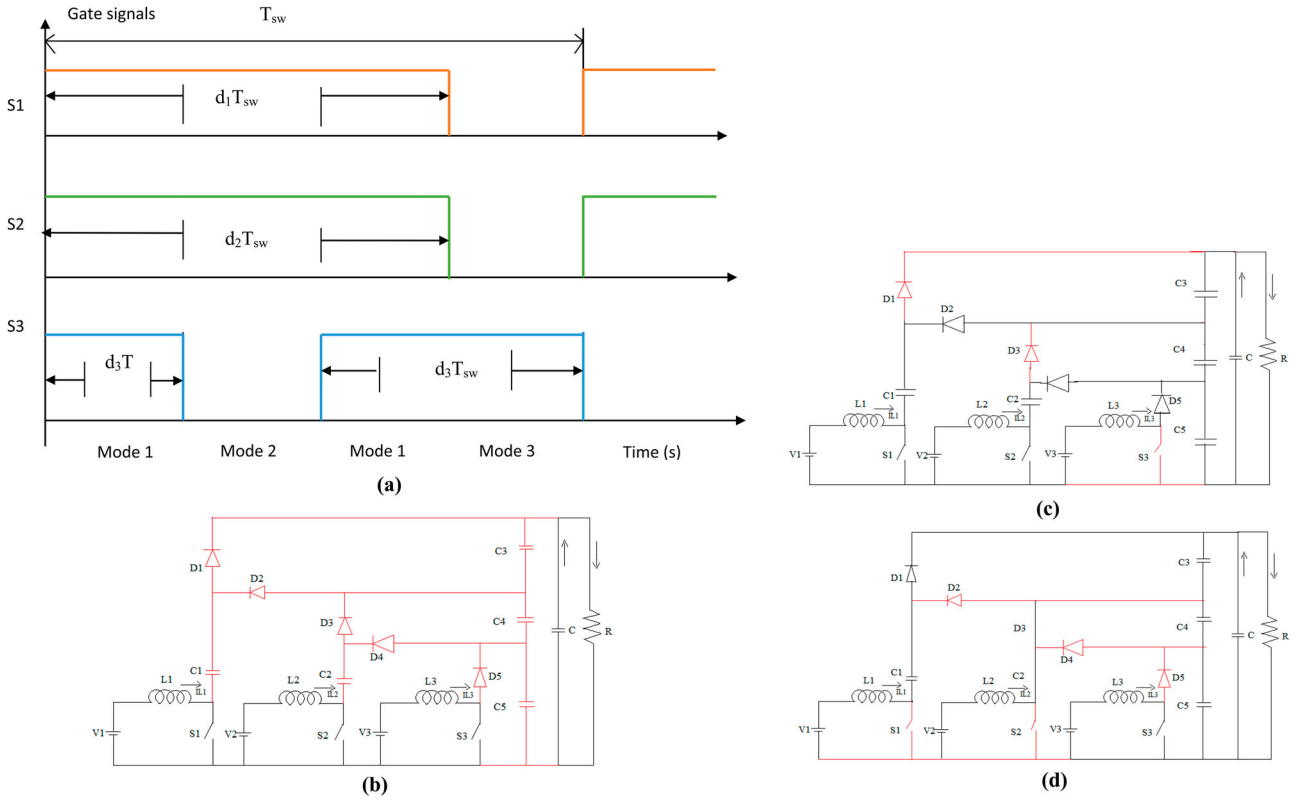

Figure 6. (a) Gating signals for switch S1, S2 and S3; (b) mode 1 operation; (c) mode 2 operation; and (d) mode 3 operation.

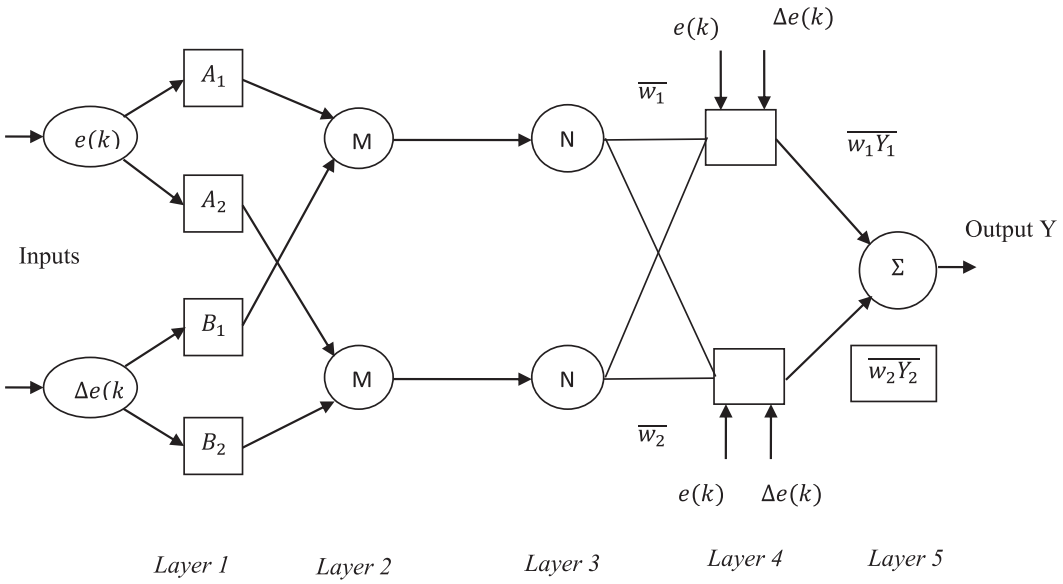

Figure 7. Structure of ANFIS DC link voltage controller.

$$i_{\mathrm{L3,avg}} = \frac{M}{1-d_3} I_{\mathrm{out}} \tag{8}$$

where I_{out} is the average output current and M is the voltage gain of the converter.

The boost cell inductor of a three-input step-up converter is designed similarly to that of a standard boost converter. The inductors are designed for continuous conduction mode functioning of the converter (CCM). For the CCM process of converter, the minimum rate of inductors can be computed as follows:

$$L_{1,\min} = \frac{(1-d_1)d_1V_1}{2MI_{\mathrm{out}}f_{\mathrm{sw}}} \tag{9}$$

$$L_{2,\min} = \frac{(1-d_2)d_2V_2}{2MI_{\mathrm{out}}f_{\mathrm{sw}}} \tag{10}$$

$$L_{3,\min} = \frac{(1-d_3)d_3V_3}{2MI_{\mathrm{out}}f_{\mathrm{sw}}} \tag{11}$$

Table 1. Simulation parameters of three-input sources.

Parameter	Values
WT	
Wind speed	12 m/s
Generator type	PMSG
Rated power	576 watts
Output voltage	48 V
Output current	12 A
PV panel	
Irradiance	1000 W/m^2
Temperature	25°C
Number of cells	$12 * 12 = 144$
Short circuit current (Isc)	5.33 A
Open circuit voltage (Voc)	86.7 V
Current at maximum point (Impp)	5 A
Voltage at maximum power point (Vmpp)	82 V
Maximum power (Pmpp)	410 watts
FC	
Number of cells	65
Output voltage	48 V
Output current	14.1 A
Output power	676 W

Table 2. Simulation parameters for three-input step-up converter and grid-tied inverter.

Three-input step-up converter	
Parameters	Values
Rated power	2000 watts
Inductors (L1, L2, and L3)	1 mH
Duty cycles of the switches	0.6
Capacitors (C1, C2, C3)	10 mF
Switching frequency (f_{sw})	10 kHz
Output voltage	515 V
Output current	3.89 A
Grid-tied inverter	
Grid voltage	400 V
Grid frequency	50 Hz
Filter inductor (L11)	1000 mH
Filter inductor (L22)	500 mH
Filter capacitor (C11)	100 mF
Switching frequency	10 kHz
PR controller proportional gain	8.500
PR controller integral gain	100
PR controller harmonic filter gain	986.8

where f_{sw} is the switching frequency of the converter and V1, V2, and V3 are the input voltage of each port of the converter.

The capacitor value for three-input step-up converters is given as follows:

$$C_{1,\min} = C_{2,\min} = C_{3,\min} = \frac{\lambda V_o}{f_{sw} R_{Lmin} V_{PP,max}} \quad (12)$$

The maximum ripple voltage is denoted by V_{PPmax}, and the converter's minimum load resistance is denoted R_{Lmin}. The λ value should be between 1 and 3 to account for the effect of output voltage ripple caused by the capacitors' effective series resistance.

2.5. ANFIS-based DC link voltage control

Neural networks are a family of intelligent algorithms with which they can be used to predict, classify and control time series and also for identification purposes. In those studies, it is more important to minimize the error value and thereby increase efficiency. Figure 7 shows the ANFIS structure for the DC link voltage control. The ANFIS controller receives two inputs, such as error voltage $e(k)$ and rate of change of error voltage $\Delta e(k)$, and based on these inputs and fuzzy rules created by means of the neural network, the ANFIS controller provides reference direct axis current (I_d*) to the grid inverter control. ANFIS input is described as follows:

$$e(k) = V_{dc}(\text{ref}) - V_{dc} \quad (13)$$

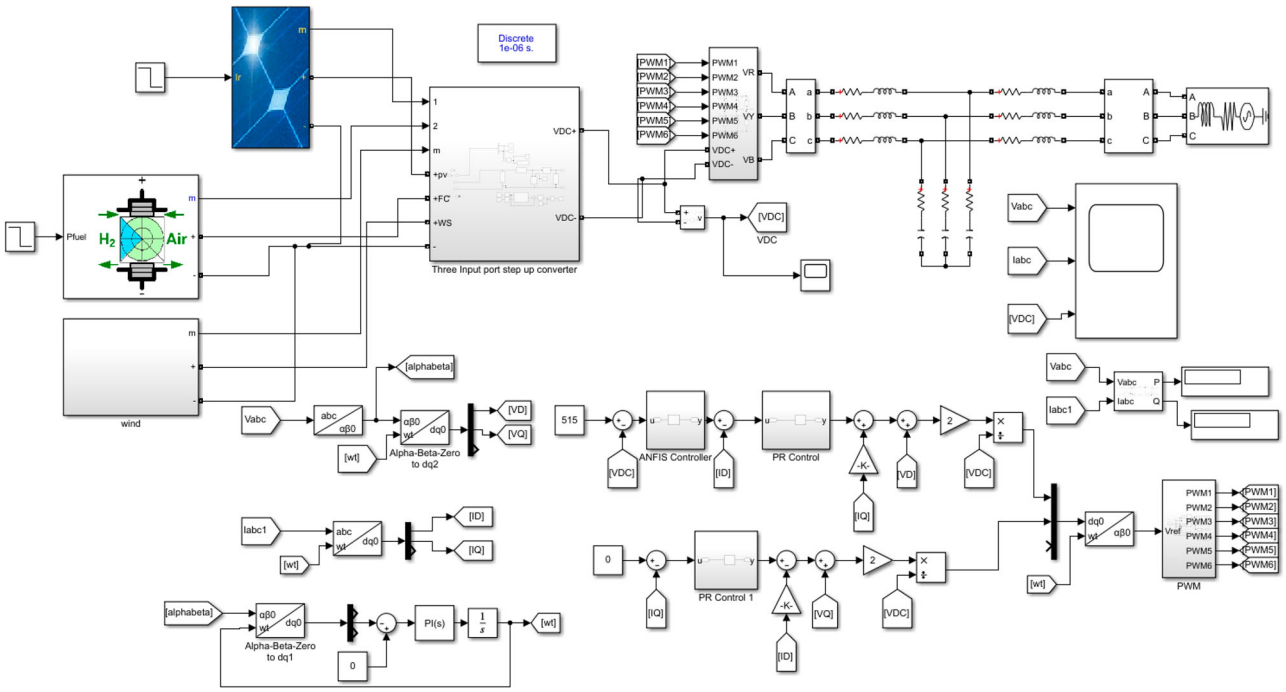

Figure 8. Simulink model of the three-input port step-up converter for hybrid energy with grid integration.

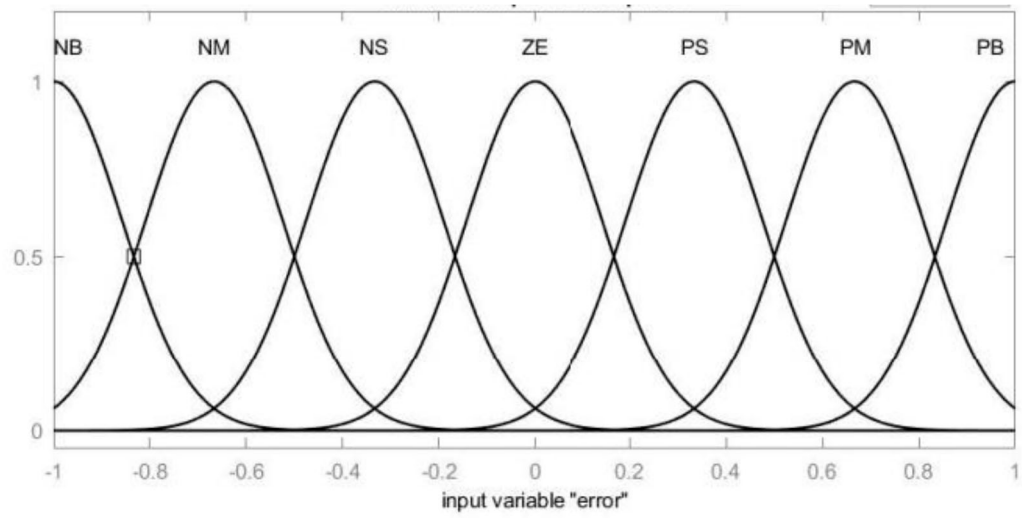

(a)

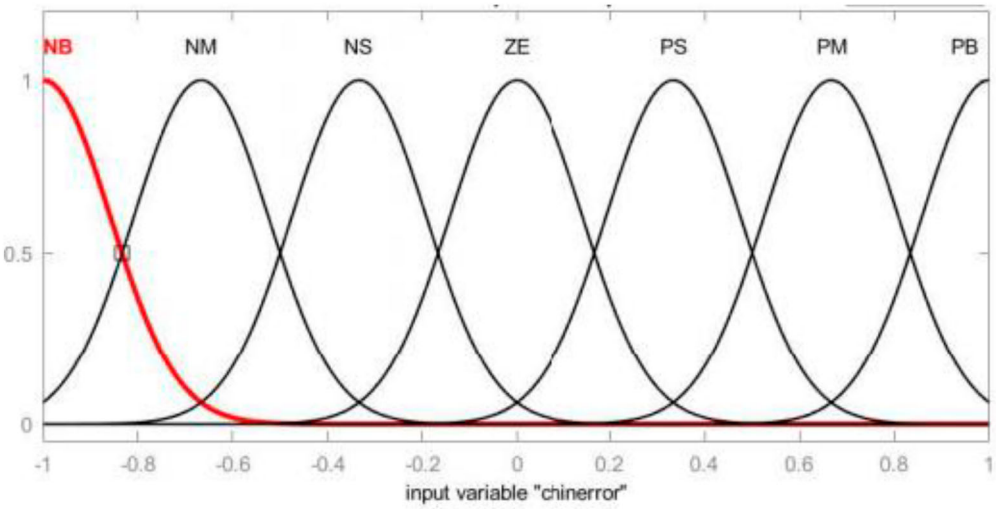

(b)

Figure 9. (a) Membership function of error voltage and (b) membership function of rate of change of error voltage.

$$\Delta e(k) = e(k) - e(k-1) \tag{14}$$

In ANFIS architecture, if-then rules are based on the first-order Sugeno model are considered.

Rule 1: If $(e(k)_1$ is $A_1)$ and $(\Delta e(k)_1$ is $B_1)$ then $(Y_1 = s_1 e(k)_1 + t_1 \Delta e(k)_1 + r_1)$

Rule 2: If $(e(k)_2$ is $A_2)$ and $(\Delta e(k)_2$ is $B_2)$ then $(Y_2 = s_2 e(k)_2 + t_2 \Delta e(k)_2 + r_2)$

where A_i and B_i denote the input fuzzy sets. The output is denoted as Y_i.

3. Simulation results and discussions

The three-input step-up converter for grid integration in a hybrid renewable energy system is simulated with MATLAB software, and the findings are reported in this part. The proposed system is made up of three sources: a WT, a PV system and a FS cell, each of which produces a different voltage and power. Table 1 shows the modelling specifications for the wind system, PV system and FC stack cell.

The simulation specification of the three-input step-up converter and grid-tied inverter is shown in Table 2.

The overall Simulink model of the three-input port step-up converter for hybrid energy with grid integration is shown in Figure 8.

The torque supplied to the generator shaft is the output of the WT simulation model, with wind and generator speeds as inputs. The torque generated by a generator is determined by its power and speed. The integrated Sim Power System library was used to create the PMSG WT model. WT drives the rotor shaft and generates mechanical torque based on the generator and wind speed. The rectifier and the three-input port step-up converters are connected to the generator's electrical output power (stator winding).

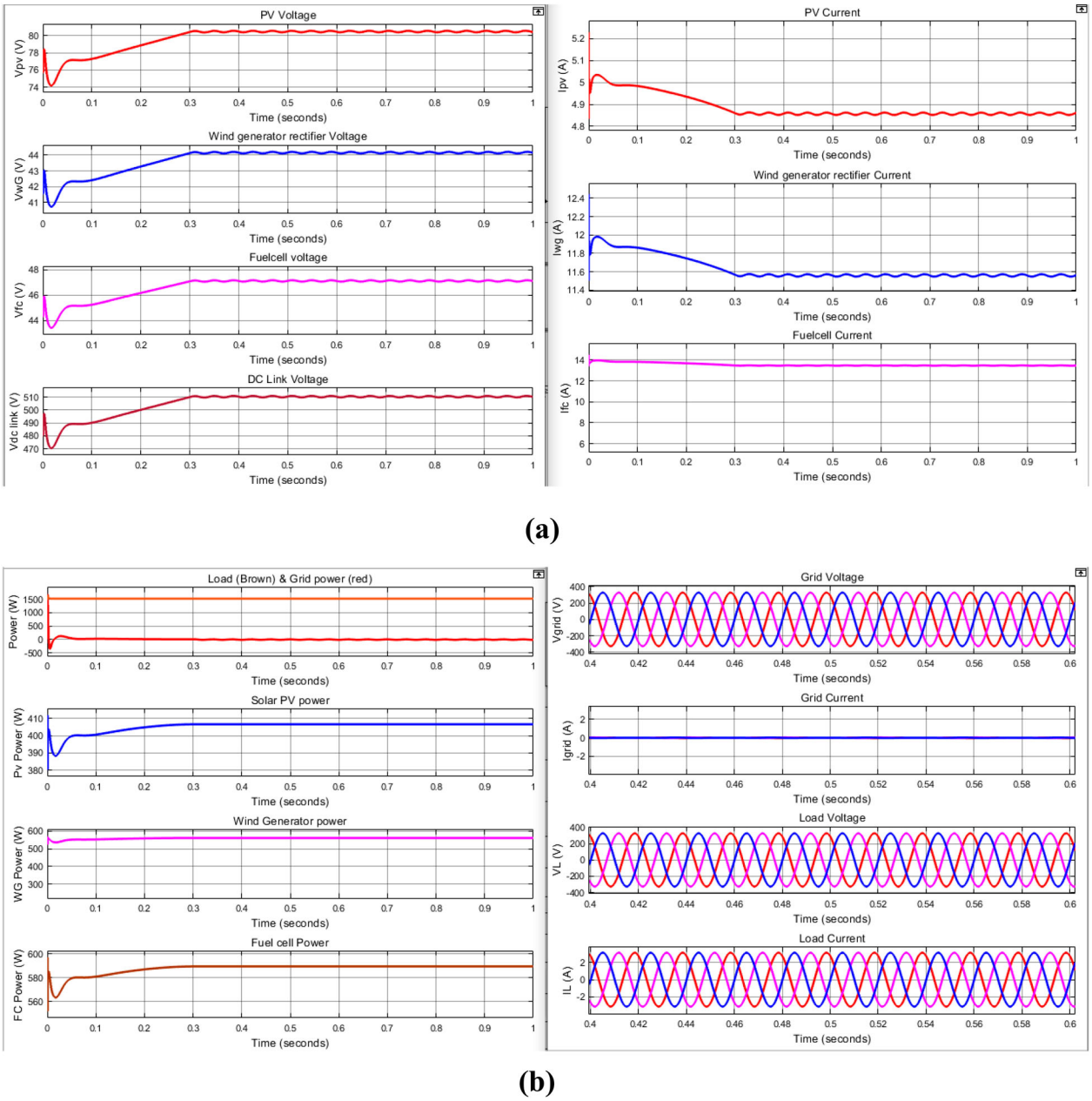

Figure 10. (a) Voltage and current for constant input parameter variation conditions with constant load and (b) power and instantaneous voltage and current for constant input parameter conditions with constant load.

PV model is created and implemented to check the non-linear properties of the PV module output. This PV model receives two inputs i.e. solar irradiance and cell temperature, to give the output as voltage and current, and it is connected to the three-input port step-up converter. FS was constructed and implemented to check the non-linear nature of the FC output. This model receives one input i.e. fuel pressure and output of the FC model is voltage and current, and it is connected to the three-input port step-up converter.

MATLAB Simulink was used to create and construct the ANFIS controller model. A fuzzy logic method with a five-layer artificial neural network (ANN) structure is used in the proposed neuro-fuzzy controller. The ANFIS system employs neural network techniques to choose an appropriate rule base, which is accomplished by a backpropagation technique. DC link voltage maintained at reference dc voltage is based on ANFIS controller output. Figure 9(a,b) shows the error and rate of change of the error voltage membership function.

The grid is connected to the load side. Initially, the total power generated by the three sources is sent to the three-input step-up DC-to-DC converter. Then, the output of converter is given to grid through inverter.

3.1. Results and discussion:

In this section, simulation results are discussed for the following operating conditions such as constant input parameter conditions with a constant load, sudden change in input parameter variations in a solar

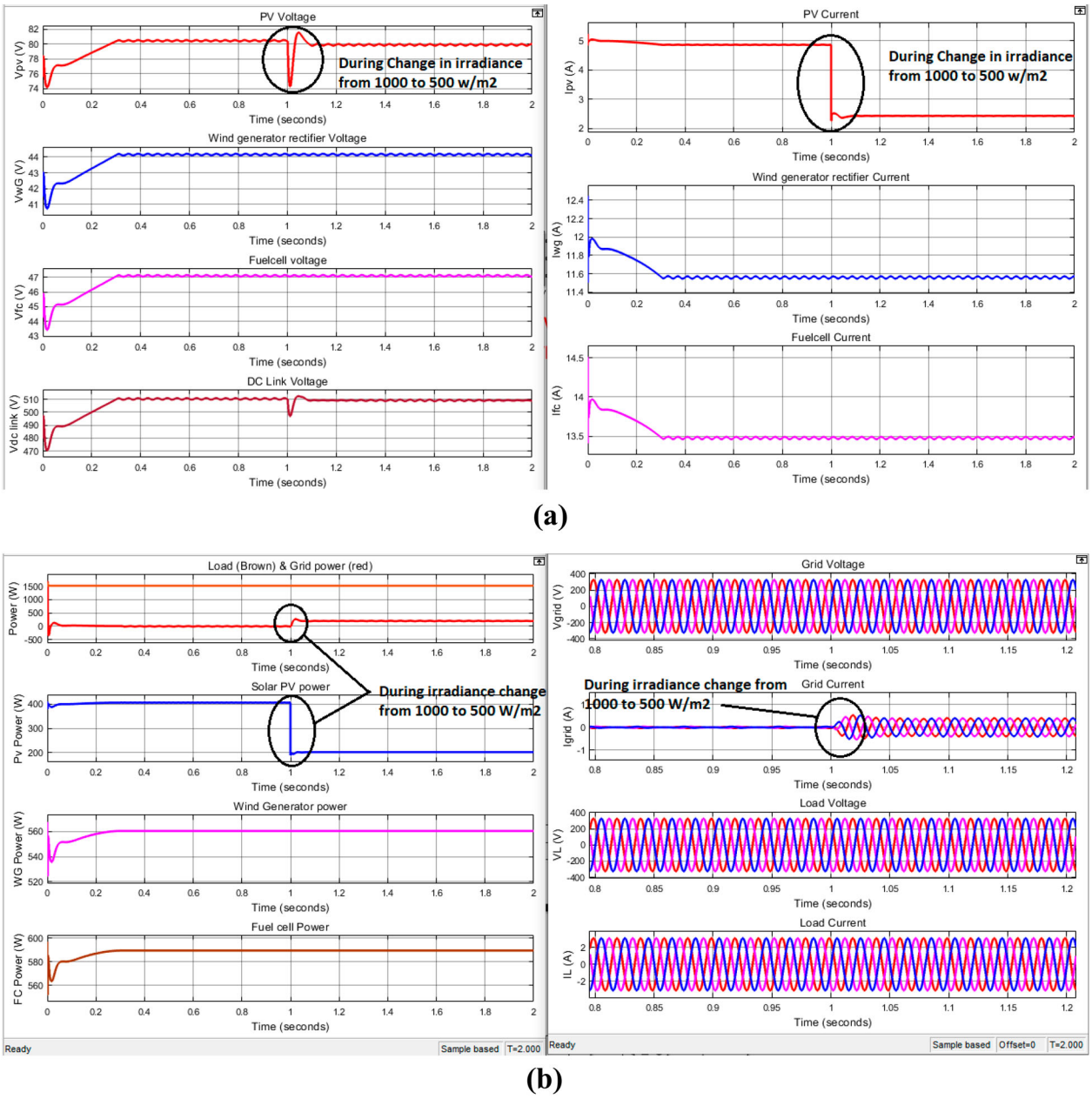

Figure 11. (a) Voltage and current for sudden change in irradiance variations in solar PV system and (b) power and instantaneous voltage and current for sudden change in irradiance variations in solar PV system.

PV system, FC system and wind energy system with a sudden change in load variation conditions.

3.1.1. Constant input parameter conditions with constant load

In these conditions, irradiance and cell temperature of the PV panel are fixed at 1000 W/m^2 and 25°C, wind speed of the WT is fixed at 12 m/s, fuel pressure of the FC stack is fixed at 1 atm and load is fixed at 1500 W. The corresponding results are shown in Figure 10(a,b).

In these conditions, PV panel voltage and current maintain at 82 V and 4.95 A; wind generator rectifier voltage and current maintain at 44 V and 11.6 A; and FC voltage and current maintain at 47 V and 13.9 A, respectively. The power generated by the PV panel, wind generator rectifier and FC stack are 406, 510.4 and 653.3 W, respectively. Total power generation by the renewable sources is 1569 watts, and it satisfies the load demand power loss in the system and grid not supplying the power to the load.

3.1.2. Sudden change in irradiance variations in solar PV system

In these conditions, irradiance of the PV panel varied from 1000 to 500 W/m^2 at 1 s, and the temperature is fixed 25°C, wind speed of the WT is fixed at 12 m/s, fuel pressure of the FC stack is fixed at 1 atm and load is fixed at 1500 W. The corresponding results are shown in Figure 11(a,b).

In these conditions, PV panel voltage and current maintain at 80 V and 2.45 A, wind generator rectifier voltage and current maintain at 44 V and 11.6 A and

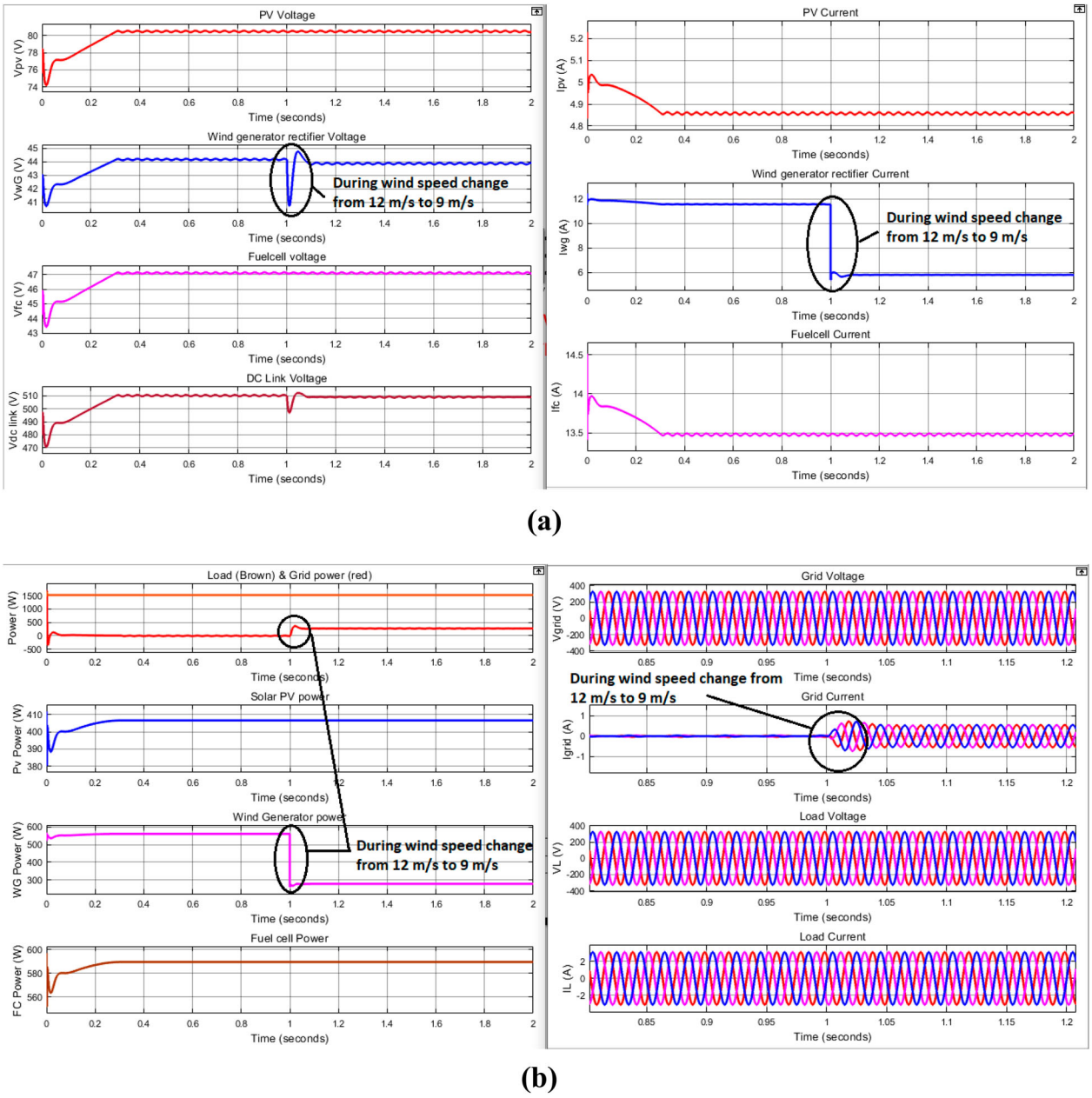

Figure 12. (a) Voltage and current for sudden change in wind speed condition of the WT and (b) power and instantaneous voltage and current for sudden change in wind speed condition of the WT.

FC voltage and current maintain at 47 V and 13.9 A, respectively. The power generated by the PV panel, wind generator rectifier and FC stack are 196, 510.4 and 653.3 W, respectively. Total power generation by the renewable sources is 1359 watts and grid supplying 200 W power to satisfy the load demand and power loss in the system.

3.1.3. Sudden change in wind speed condition of the WT

In these conditions, irradiance and cell temperature of the PV panel are fixed at 1000 W/m^2 and 25°C, wind speed of the WT is varying from 12 to 9 m/s at 1 s, fuel pressure of the FC stack is fixed at 1 atm and load is fixed at 1500 W. the corresponding results are shown in Figure 12(a,b).

In these conditions, PV panel voltage and current maintain at 82 V and 4.95 A, wind generator rectifier voltage and current maintain at 44 V and 6.36 A and FC voltage and current maintain at 47 V and 13.9 A. The power generated by the PV panel, wind generator rectifier and FC stack are 406, 280 and 653.3 W, respectively. Total power generation by the renewable sources is 1339 watts and grid supplying 260 W power to satisfy the load demand and power loss in the system.

3.1.4. Sudden change in fuel pressure of the FC

In these conditions, irradiance and cell temperature of the PV panel is fixed at 1000 W/m^2 and 25°C, wind speed of the WT is fixed at 12 m/s, fuel pressure of the FC stack varied from 1 to 0.5 atm at 1 s, and load is

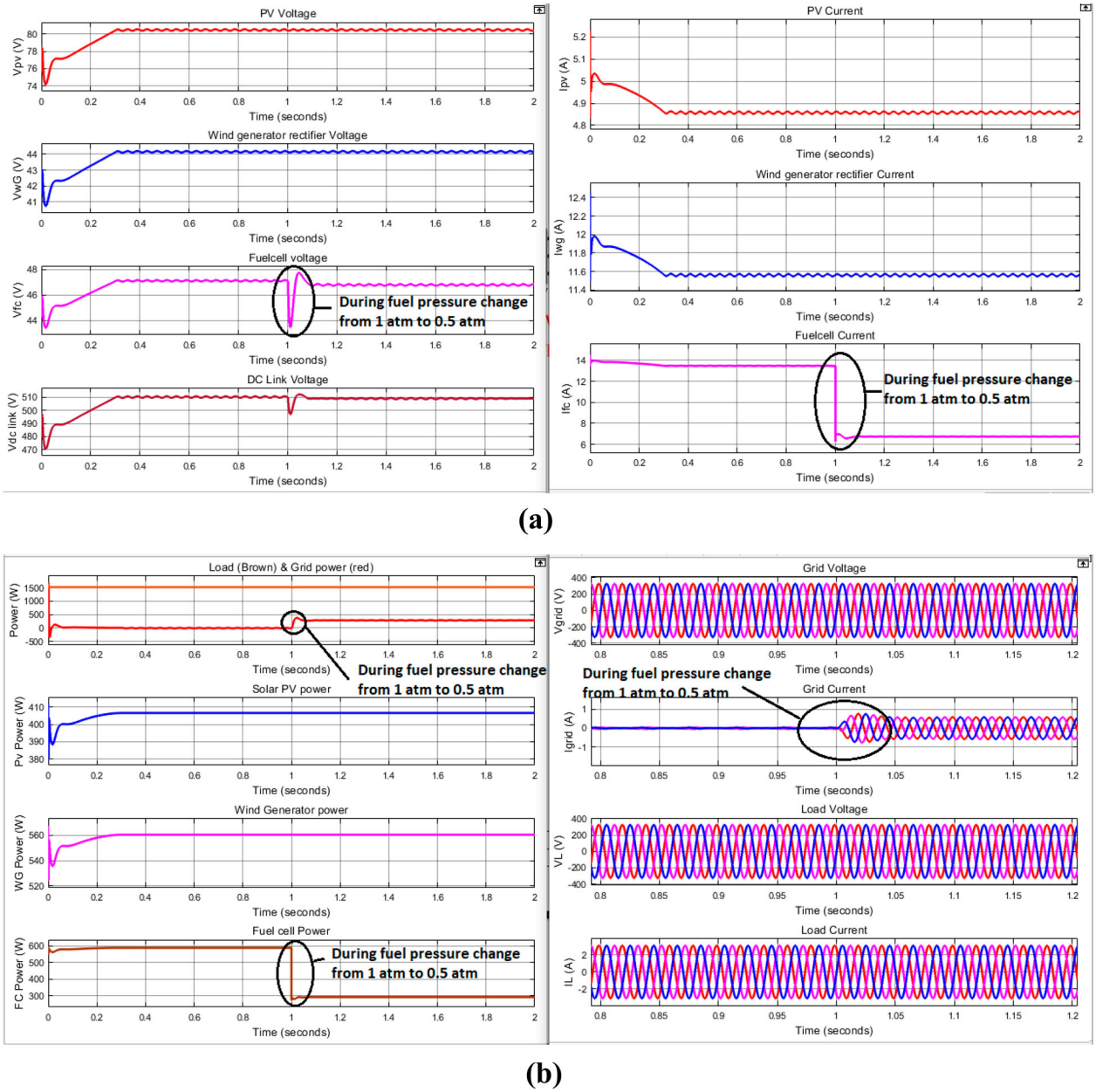

Figure 13. (a) Voltage and current for sudden change in fuel pressure of the FC and (b) power and instantaneous voltage and current for sudden change in fuel pressure of the FC.

fixed at 1500 W. the corresponding results are shown in Figure 13(a,b).

In these conditions, PV panel voltage and current maintain at 82 V and 4.95 A, wind generator rectifier voltage and current maintain at 44 V and 11.6 A, FC voltage and current maintain at 47 V and 6.19 A. The power generated by the PV panel, wind generator and FC stack are 406, 510.4 and 291 W, respectively. Total power generation by the renewable sources is 1207 watts and grid supplying 290 W power to satisfy the load demand and power loss in the system.

3.1.5. Sudden change in load conditions

In these conditions, irradiance and cell temperature of the PV panel is fixed at 1000 W/m^2 and 25°C, wind speed of the WT is fixed at 12 m/s, fuel pressure of the FC stack is fixed at 1 atm, and load demand is varied from 1500 to 1000 W. The corresponding results are shown in Figure 14(a,b).

In these conditions, PV panel voltage and current maintain at 82 V and 4.95 A, wind generator rectifier voltage and current maintain at 44 V and 11.6 A, FC voltage and current maintain at 47 V and 13.9 A. The power generated by the PV panel, wind generator rectifier and FC stack are 406, 510.4 and 653.3 W, respectively. Total power generation by the renewable sources is 1569 watts and grid receiving power 500 W from renewable energy source and remining power satisfy the load demand and power loss in the system.

3.1.6. Efficiency of the proposed system

Power efficiency is defined as the ratio of the output power to the input power. Figure 15 represents the efficiency comparison of the existing and the proposed

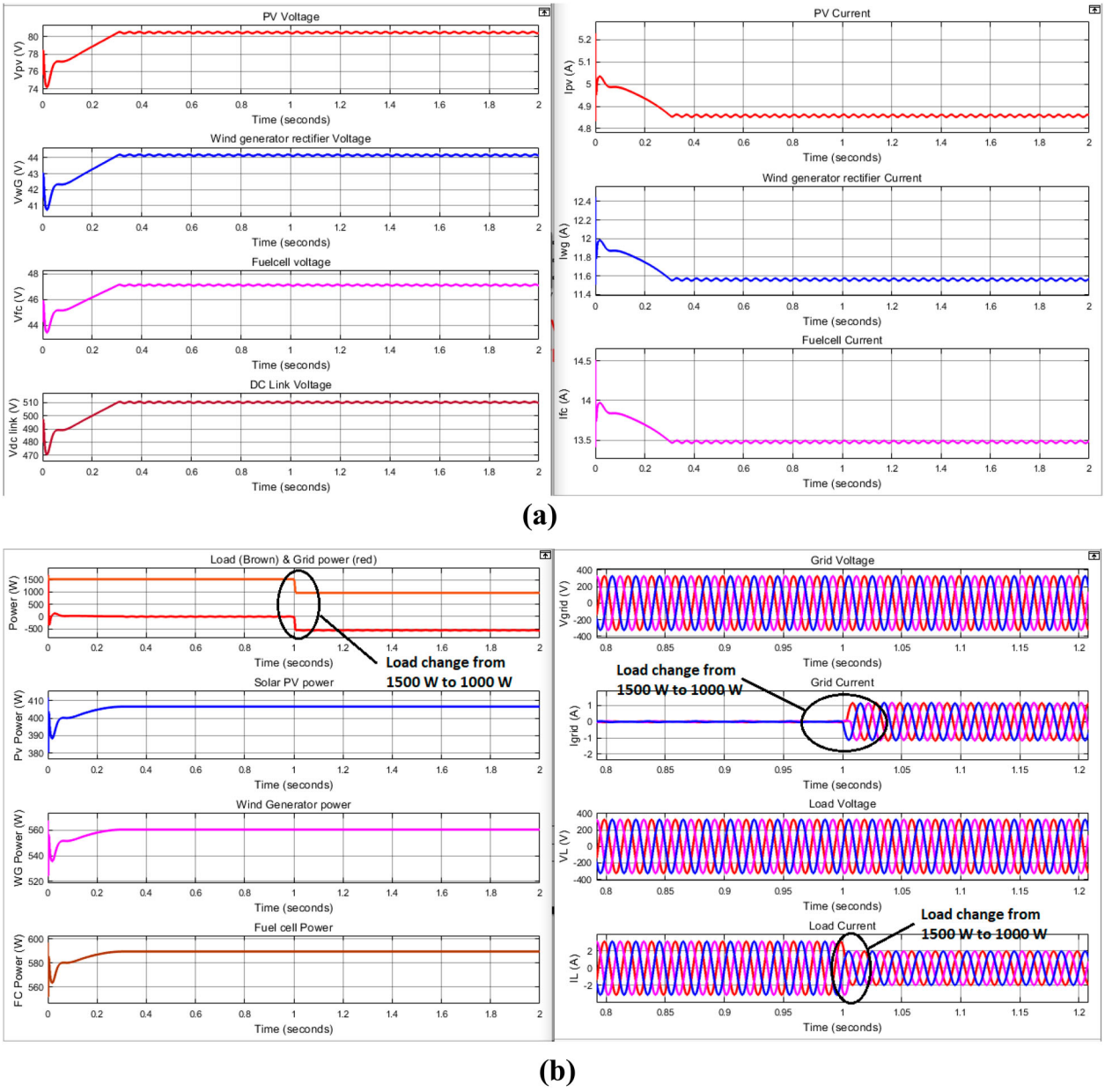

Figure 14. (a) Voltage and current for sudden change in load conditions and (b) power and instantaneous voltage and current for sudden change in load conditions.

system.

$$\eta = P_{\text{out}}/P_{\text{in}} \cdot 100\%$$

where η is the efficiency in per cent (%), P_{in} is the input power from sources (W) and P_{out} is the output power in watts (W).

The input power from the three sources is 1569 W and the output power is 1541 W. Then, the efficiency of the proposed system is

$$\eta = \frac{1541}{1569} \times 100$$

$$\eta = 98.21\%$$

Efficiencies of various converters used along with hybrid renewable energy grid-connected system are compared in Table 3 showing that the proposed converter for the hybrid system is efficient and is displayed using a bar graph. Table 3 shows the comparison between various converters.

From the above comparison on efficiencies of various DC–DC converters using hybrid inputs (three inputs), the proposed system operates with an efficiency of 98.21%.

Table 3. Efficiency comparison of various converters.

REF	Converters	Efficiency
[24]	Multiphase DC–DC converter	85%
[18]	Multi-input CBBVSI	92.4%
[8]	Single input CBBVSI	93%
[23]	Two input step-up DC–DC converter	97%
	Proposed three-input step-up DC–DC converter	98.21%

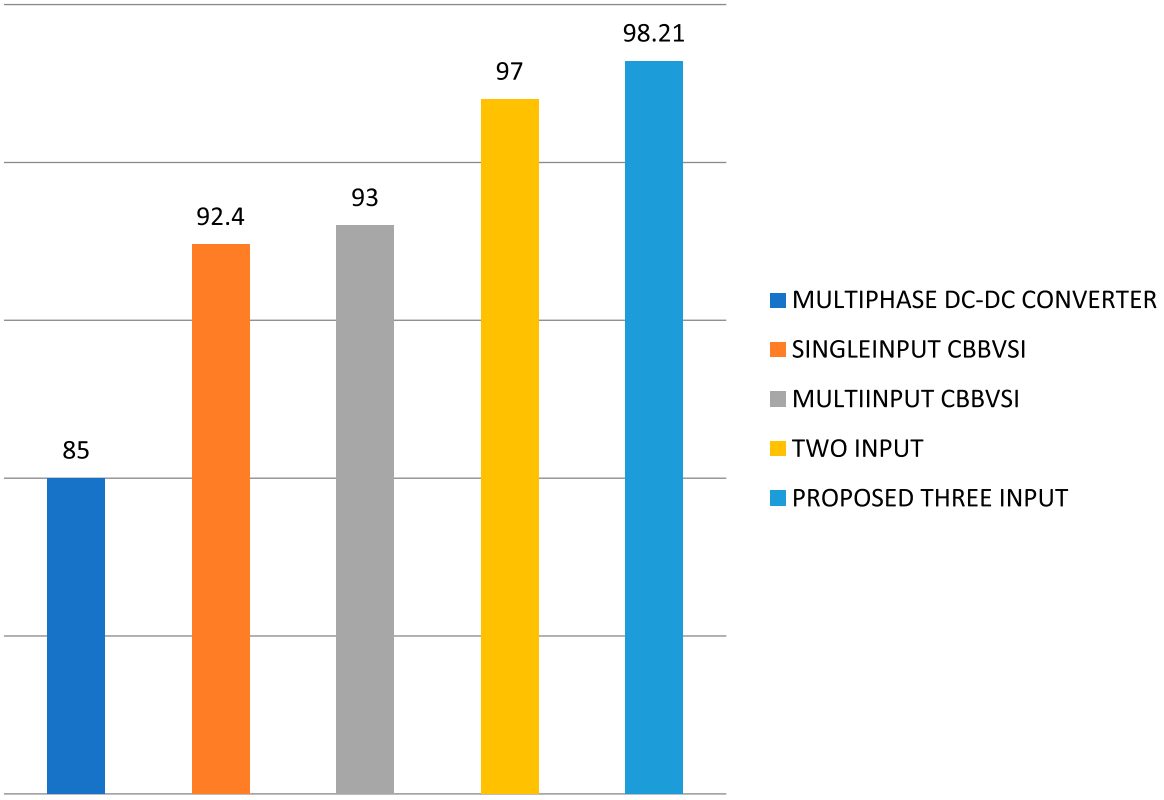

Figure 15. Efficiency comparison of the existing and proposed system.

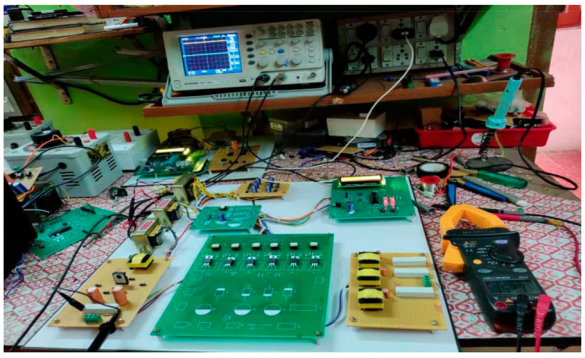

Figure 16. Hardware setup of the three-input step-up converter for hybrid renewable energy application with grid integration.

Table 4. Specification of PV, WT and FC emulator.

PV emulator	
Short circuit current	5.33 A
Open circuit voltage	86.7 V
Current at maximum power point	A
Voltage at maximum power point	82 V
Power at maximum power point	410 W
WT emulator	
Rated power	500 W
Rated current	10.4 A
Rated voltage	48 V
FC emulator	
Rated power	600 W
Rated current	12.5 A
Rated voltage	48 V

4. Experimental verification

The real-time investigation of three-input port step-up converter for hybrid renewable energy with grid integration is discussed in the section. The experimental set-up for the proposed system is shown in Figure 16. PV emulator, WT emulator and FC emulator are acted as renewable energy sources, and the specification of the emulators is presented in Table 4. Specification for the three-input port step-up converter and grid-tied inverter are same as the simulation specification.

In this section, experimental results are discussed for the following operating conditions such as constant input parameter conditions with constant load. In these conditions, irradiance and cell temperature of the PV emulator is fixed at 1000 W/m^2 and 25°C, wind speed of the WT emulator is fixed at 12 m/s, fuel pressure of the FC emulator is fixed at 1 atm, and load is fixed at 1150 W. the corresponding results are shown in Figure 17. In these conditions, PV Emulator voltage and current are maintained at 80 V and 4.2 A, wind emulator voltage and current maintain at 48 V and 9.1 A, FC voltage and current maintain at 48 V and 11.5 A. The power generated by the PV panel, wind generator rectifier and FC stack are 336, 437 and 437 W, respectively. Total power generation by the renewable sources is 1210 watts, and it satisfies the load demand power loss in the system and grid not supplying the power to the load.

Experimental results for change irradiance from 1000 to 500 W/m^2 are shown in Figure 18.

In these conditions, PV Emulator voltage and current maintain at 80 V and 4.2 A during 1000 W/m^2, PV

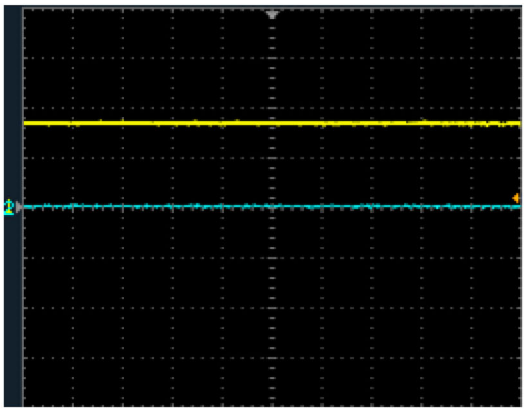

PV Emulator Voltage (X axis – 10 ms/div & Y axis – 50 V/div)

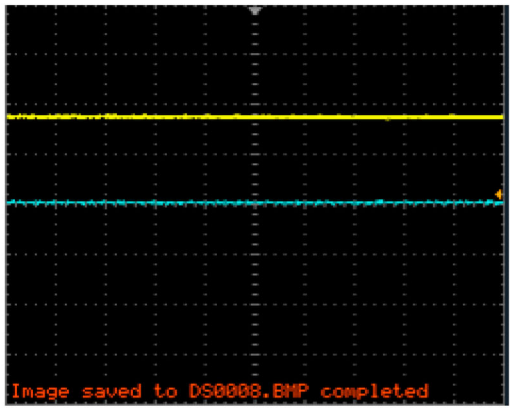

Wind turbine Emulator Voltage (X axis – 10 ms/div & Y axis – 25 V/div)

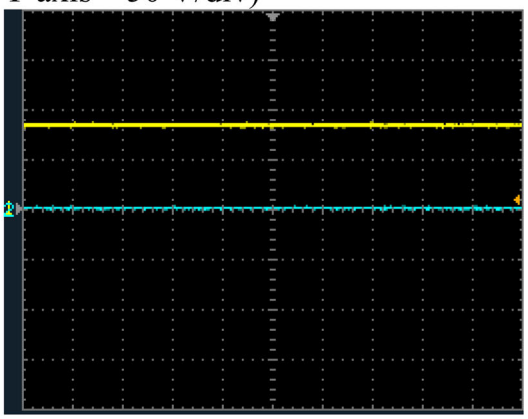

Fuel cell Emulator Voltage (X axis – 10 ms/div & Y axis – 25 V/div)

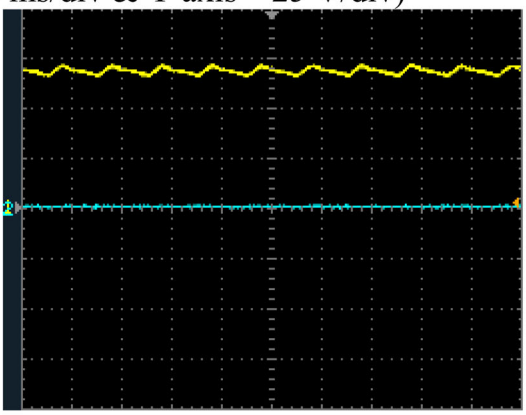

Converter output voltage (X axis – 10 ms/div & Y axis – 200 V/div)

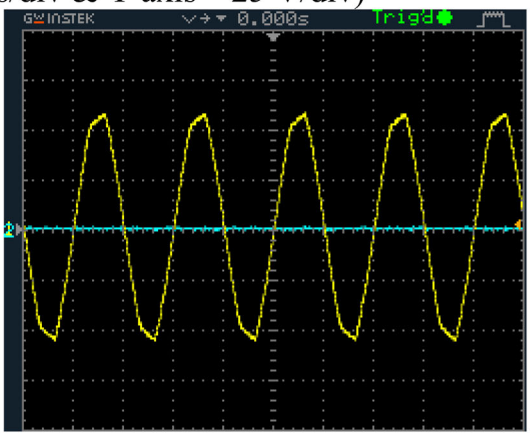

Load Voltage (X axis – 10 ms/div & Y axis – 150 V/div)

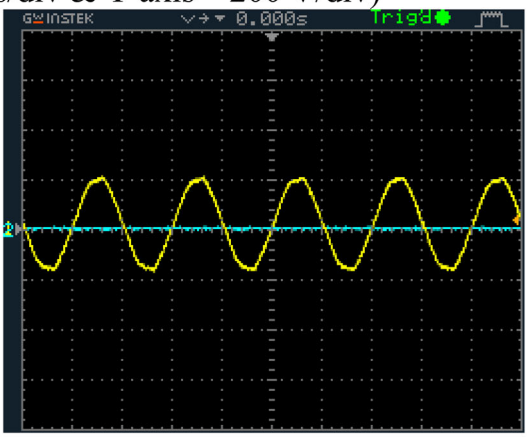

Load Current (X axis – 10 ms/div & Y axis – 5 A/div)

Figure 17. Instantaneous voltage and current for constant input parameter with constant load condition.

panel voltage maintains at 75 V and 2 A when irradiance changes to 500 W/m^2. During these conditions, grid current changes from 0.1 to 2.12 A due to power fall in the PV panel due to reduction in irradiance. During the change in irradiance condition, also power balance is maintained between source and load.

5. Conclusion

A new extensible three-input step-up DC–DC converter is designed in this work to achieve better voltage gain. The suggested converter improves voltage by increasing the number of inputs, making it appropriate for a wide range of applications in hybrid energy systems, from low to high voltage/power (HESs). The overall system has been implemented in MATLAB software. The proposed system was tested in MATLAB with different operating conditions such as constant input parameter with constant load conditions, sudden change in irradiance of PV panel, sudden change in wind speed conditions of WT, sudden change in fuel pressure conditions of FC and sudden change in load

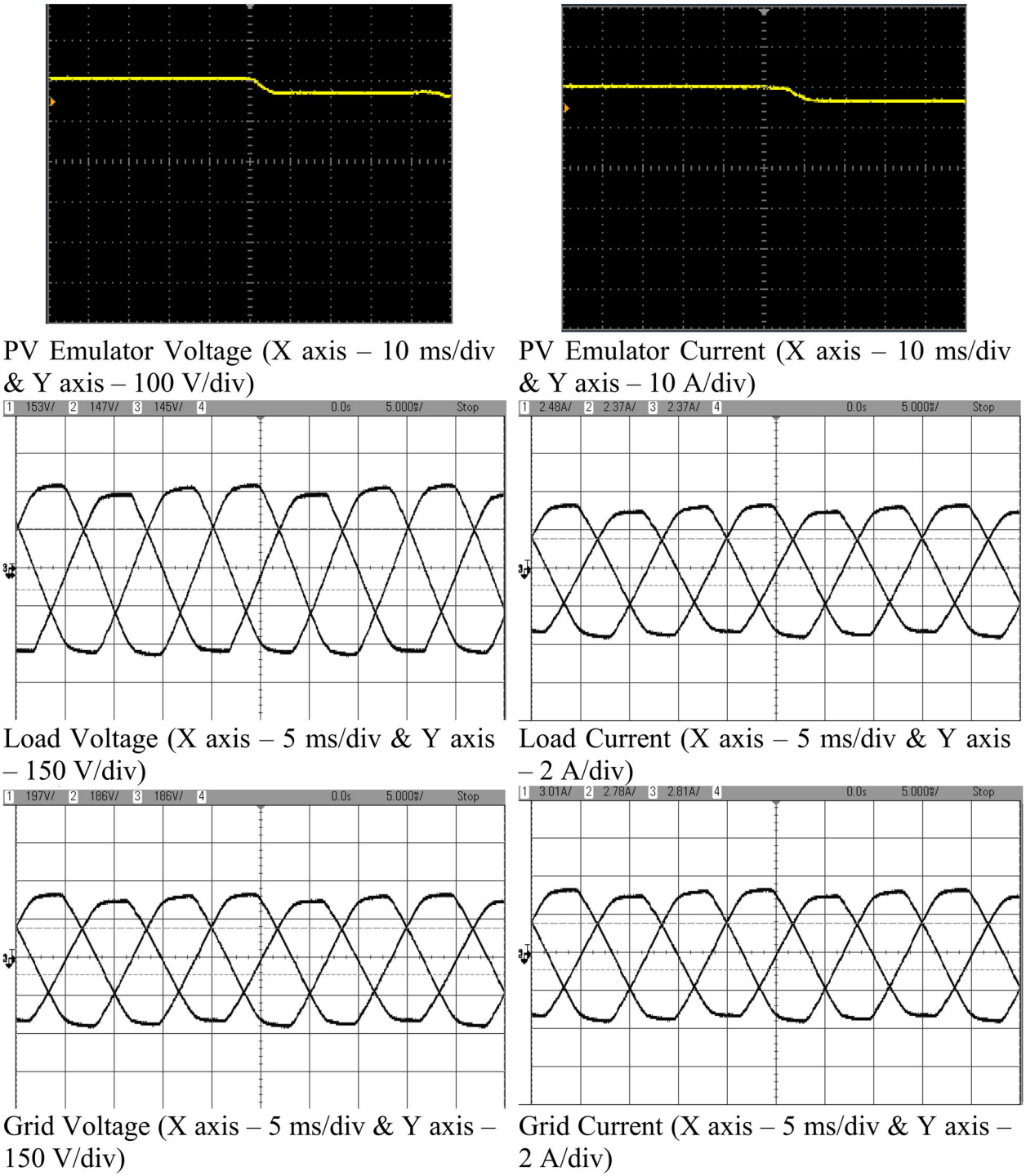

Figure 18. Instantaneous voltage and current for change irradiance from 1000 to 500 W/m^2.

conditions, resulting in the maintenance of power balance in all-operating conditions. In simulation, the proposed system converter efficiency is around 98.21% for the all-operating conditions. The proposed system has been investigated in real-time hardware experimentation. From these test results, the proposed converter can act as a high step-up multi-input converter for hybrid renewable energy applications.

Disclosure statement

No potential conflict of interest was reported by the author(s).

Funding

The author(s) reported there is no funding associated with the work featured in this article.

References

[1] Kemabonta T, Kabalan M. Integration of renewable energy resources from the perspective of the midcontinent independent system operator: a review. Electr J. 2018;31(9):28–33.
[2] Wu G, Ruan X, Ye Z. Nonisolated high step-up dc–dc converters adopting switched-capacitor cell. IEEE Trans Indus Electron. 2015;62(1):383–393.

[3] Liang T-J, Lee J-H, Chen S-M, et al. Novel isolated high-step-up DC–DC converter with voltage lift. IEEE Trans Indus Electron. 2013;60(4):1483–1491.
[4] Saravanan S, Babu NR. RBFN based MPPT algorithm for PV system with high step up converter. Energy Convers Manag. 2016;122:239–251.
[5] Saravanan S, Babu NR. Non-isolated DC-DC converter for renewable based grid application. Energy Procedia. 2016;103:310–315.
[6] Zhang N, Sutanto D, Muttaqi KM. A review of topologies of three-port DC–DC converters for the integration of renewable energy and energy storage system. Renew Sustain Energy Rev. 2016;56:388–401.
[7] Khosrogorji S, Ahmadian M, Torkaman H, et al. Multi-input DC/DC converters in connection with distributed generation units – a review. Renew Sustain Energy Rev. 2016;66:360–379.
[8] Mohammed SA, Dogan H, Ozgun MT. An 85%-efficiency reconfigurable multiphase switched capacitor DC-DC converter utilizing frequency, switch size, and interleaving scaling techniques. Microelectronics J. 2017;67:155–161.
[9] Hossain MZ, Rahim NA. Recent progress and development on power DC-DC converter topology, control, design and applications: a review. Renew Sustain Energy Rev. 2018;81:205–230.
[10] Nejabatkhah F, Danyali S, Hosseini SH, et al. Modeling and control of a new three-input DC–DC boost converter for hybrid PV/FC/battery power system. IEEE Trans Power Electron. 2012;27(5):2309–2324.
[11] Danyali S, Hosseini SH, Gharehpetian GB. New extendable single-stage multi-input DC-DC/AC boost converter. IEEE Trans Power Electron. 2014;29(2):775–788.
[12] Caroa JCR, Maldonado JCM, Gonzalez AV, et al. DC-DC multiplier boost converter with resonant switching. Electr Power Syst Res. 2015;115:83–90.
[13] Nouri T, Hosseini SS, Babaei E, et al. A non-isolated three-phase high step-up DC-DC converter suitable for renewable energy systems. Electr Power Syst Res. 2016;140:209–224.
[14] Parastar A, Ghandomkar A, Seok J-K. High-efficiency multilevelflying-capacitor DC/DC converter for distributed renewable energy systems. IEEE Trans Ind Electron. 2015;62(12):7620–7630.
[15] Leva S, Zaninelli D. Hybrid renewable energy-fuel cell system: design andperformance evaluation. Electr Power Syst Res. 2009;79(2):316–324.
[16] Matsuo H, Kurokawa F, Byunghoon L, et al. Suppression of the input current harmonics and output voltage ripple using the novel multiple-input ac-dc converter. In: Proc. IEEE 19th Telecommunications Energy Conference; 1997. p. 710–714.
[17] Matsuo H, Wenzhong L, Kurokawa F, et al. Characteristics of the multiple-input dc-dc converter. IEEE Trans Ind Electron. 2004;51:625–631.
[18] Usmani MJ, Haque A, Kurukuru VSB, et al. Power management for hybrid energy storage system in electric vehicles. In: 2019 International Conference on Power Electronics, Control and Automation (ICPECA); 2019. p. 1–6. DOI:10.1109/ICPECA47973.2019.8975530
[19] Arun Raj Kumar KP, Sreedevi ML, Mineeshma GR, et al. Hybrid energy storage system interface for electric vehicles. In: 2020 IEEE International Conference on Power Electronics, Smart Grid and Renewable Energy (PESGRE2020); 2020. p. 1–6. DOI:10.1109/PESGRE45664.2020.9070367
[20] Solero L. Performance of a 10 kW power electronic interface for combined wind/PV isolated generating systems. In: Proc. IEEE PESC'96; 1996. p. 1027–1032.
[21] Caricchi F. Testing of a new dc-dc converter topology for integrated wind-photovoltaic generating systems. In: Proc. European Conf. Power Electronics and Applications; 1993. p. 83–88.
[22] Hintz A, Prasanna UR, Rajashekara K. Novel modular multiple input bidirectional DC–DC power converter (MIPC) for HEV/FCV application. IEEE Trans Ind Electron. 2015;62(5):3163–3172.
[23] Deihimi A, Mahmoodieh MES, Iravani R. A new multi-input step-up DC-DC converter for hybrid energy systems. Electr Power Syst Res. 2017; 149:111–124. ISSN 0378-7796. DOI:10.1016/j.epsr.2017.04.017
[24] Dobbs BG, Chapman PL. A multiple-input dc-dc converter. IEEE Power Electron Lett. 2003;1(1):6–9.